COBEM 2021 26th International Congress of Mechanical Engineering
November 22-26, 2021, Virtual Congress, Brazil

COB-2021-1128
PREDICTION OF AERODYNAMIC NOISE GENERATED BY CYLINDERS IN UNIFORM FLOW USING OPENFOAM

Julio Victor Vieira Martins Chadlvski
Filipe Dutra da Silva
TEG - Thermofluids Engineering Group, Universidade Federal de Santa Catarina (UFSC), Joinville, Santa Catarina
julio.chadlvski@teg.ufsc.br, filipe.dutra@teg.ufsc.br

Abstract. *Airframe noise is one of the main components of aircraft noise, especially during the approach procedure. This component is generated by the interaction of flow with aircraft elements such as high lift devices and landing gears. In this sense, the use of numerical tools became interesting for the design process as well as providing complementary data to experiments, such as flow field data in regions where measurements are difficult. The sound generation is usually computed by means of time-dependent simulations of the turbulent flow field, whereas the propagation can be considered analytically, by using acoustic analogies. The objective of this work is to build and validate a simulation model for the prediction of generated from the flow over blunt bodies, using the open-source code OpenFOAM coupled with acoustic prediction codes available in the literature. Some well-known benchmark cases were selected: an isolated cylinder and tandem cylinders in uniform flow. Three-dimensional incompressible Unsteady Reynolds Averaged Navier-Stokes simulations were conducted using the SST turbulence model. The acoustic field is computed using both Curle's analogy and Ffowcs-Williams and Hawkings analogy with permeable surface formulation. The results of the simulations, both the flow and the acoustic field, are compared with experimental data available in the literature. Mean flow results show reasonable agreement with the reference experimental data. For the acoustic field, numerical results showed good agreement with experimental data for the tandem cylinder case, while presenting higher discrepancies relative to experiments for the isolated cylinder case.*

Keywords: *Airframe Noise, Computational Aeroacoustics, OpenFOAM*

1. INTRODUCTION

An important source of aircraft noise is airframe noise, which is more significant during approach and landing. This noise component is generated by the interaction of turbulent flow with surfaces of the airplane, such as landing gears, trailing edges and airframe cavities (Ruijgrok, 1993). Usually, airframe noise can be predicted using computational aeroacoustics tools, in particular, hybrid methods are employed due to their ability to provide accurate results with low computational cost, when compared to the direct noise computation.

In this paper, a numerical hybrid method approach was employed to calculate the far-field noise due to flow-induced sound over blunt bodies. In such approach, sound generation and sound propagation are treated separately. Near-field aerodynamic perturbations that generate noise are calculated by Computational Fluid Dynamics (CFD) methods, while the far-field noise can be obtained by analytical acoustic analogies using the near-field flow data as input.

The noise generated by the flow over a circular cylinder is a benchmark problem in computational aeroacoustics, and has been studied by several authors. Ergin and Bulut (2017) simulated the flow over a two-dimensional cylinder, with Reynolds number (Re) of 90,000, using incompressible Unsteady Reynolds Averaged Navier-Stokes (URANS) equations with k-ω Shear Stress Transport (SST) turbulence model. Noise was calculated using the Ffowcs Williams and Hawkings (FW-H) analogy and with a sound model based on Proudman analogy. Orselli *et al.* (2009) also performed incompressible simulations with Re = 90,000 based on experimental studies of Revell *et al.* (1978). Both a two-dimensional approach, using URANS models, and a three-dimensional approach, using Large Eddy Simulation (LES), were used. In both approaches the far-field noise was computed using FW-H analogy. After applying the correction methods proposed by Kato *et al.* (1993) and Seo and Moon (2007), which are used to account for different span lengths between the numerical and experimental results, the 3D LES simulation showed good agreement with experimental data.

The flow over circular cylinders in tandem arrangement is also designated as a benchmark for aeroacoustic and wake interference problems. Zdravkovich (1985) studied different distances between both cylinders and verified a dependence of the oscillations induced by vortex shedding with the cylinder arrangement. Lockard *et al.* (2007) provides flow and acoustic data for a tandem cylinders configuration, separated by a distance 3.7 diameters, from experimental and numerical tests with $Re = 1.66 \times 10^5$. Results showed that downstream cylinder is the main responsible for noise radiation.

In this work, simulation models were built, using open-source codes, to predict the aerodynamic and acoustic fields from an isolated circular cylinder and tandem cylinders in uniform flow. Validation is conducted by comparing results with experimental data available in literature. The used software was the open-source CFD code OpenFOAM (OpenCFD, 2020). Far-field noise was calculated using the Ffowcs Williams and Hawkings (FW-H) acoustic analogy implemented in a library coupled with OpenFOAM, developed by Epikhin *et al.* (2015), known as libAcoustics. The paper is structured as follows: section 2 describe the used geometries, methods and computational setup; section 3 present the results for both benchmark cases, and finally, section 4 presets the main conclusions.

2. METHODOLOGY

2.1 Flow-field simulations

As aforementioned, we adopted two benchmark cases for this study: and isolated cylinder and two cylinders in tandem arrangement. Geometry and flow conditions for the isolated cylinder were based on the experiments conducted by Revell *et al.* (1978), in which cylinders of two different diameters were tested, one with 19 mm and the other with 38 mm, both with a spanwise length of 0.48 cm. Tests considered Reynolds numbers between 45,000 and 450,000, and Mach numbers between 0.1 and 0.5. Far-field noise was measured by microphones located at a distance of 2.348 m from the center of the cylinder at different polar angles.

The tandem cylinders setup was based on Lockard *et al.* (2007) and Jenkins *et al.* (2005) experiments, executed, respectively, in the Quiet Flow Facility (QFF) and in the Basic Aerodynamic Research Tunnel (BART) at NASA Langley Research Center. The arrangement is composed of two aligned cylinders with diameter $D = 5.71$ cm and span length of $12.4D$, separated by a distance of $3.7D$. The experiments considered a Reynolds number of 166,000 with Mach number 0.127. For far-field noise measurements three microphones were located at different positions from the center of the upstream cylinder, which x and y coordinates are: $[-8.33D, 27.815D]$, $[9.11D, 32.94D]$ and $[26.55D, 27.815D]$.

The defined computational domains are similar for both validation cases and their schematic is depicted in Figure 1, showing the boundaries and the cylinder walls. For the one-cylinder case, only the blue cylinder is included, whereas for the tandem arrangement, both blue and gray cylinders are present.

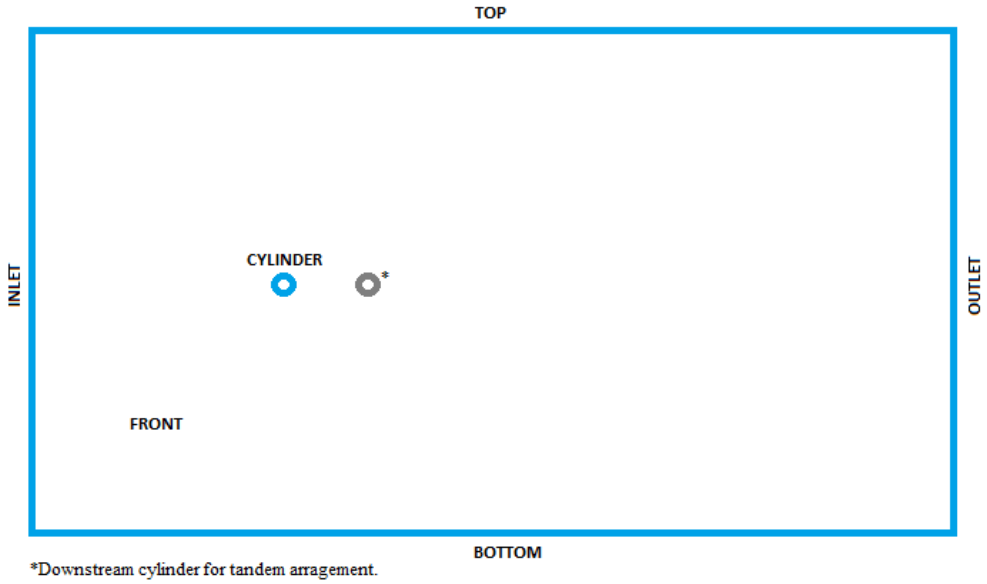

Figure 1: Schematic of the used computational domain.

In both proposed cases, the flow field was computed with incompressible URANS simulations in OpenFOAM v2012, using the k-ω SST turbulence model (Menter, 1994), considering a three-dimensional computational domain. For the gradient terms, a Multi-directional cell-limited scheme was adopted, while a second order linear upwind scheme was used for the advective terms. To solve the pressure-velocity coupling the Pressure-Implicit with Splitting of Operators (PISO) algorithm was used.

Regarding boundary conditions, a free-stream velocity condition with a free-stream gauge pressure of 0 Pa was imposed at the inlet, top and bottom boundaries. For the outlet, a fixed gauge pressure of 0 Pa was prescribed with a zero-gradient condition for velocity. A no-slip wall condition was used on the cylinder surfaces and, for the front and back boundaries, a slip wall condition was imposed. The turbulence variables k and ω were defined based on a turbulence intensity of $I = 0.2\%$ and eddy viscosity ratio $\nu_t/\nu = 2$ for the isolated cylinder case, whereas for tandem cylinders case, $I = 0.1\%$ and $\nu_t/\nu = 2$ were considered.

2.2 Case A: Isolated Cylinder

In accordance with the experiments from Revell *et al.* (1978), the simulations considered an isolated cylinder with diameter $D = 38$ mm, and flow conditions corresponding to Re = 270,000 and $M = 0.3$. In order to reduce computational cost, the spanwise extension of the cylinder was reduced to $2.5D$, the same value adopted by Orselli *et al.* (2009). Inlet and outlet boundaries were located, respectively, at $14.5D$ upstream and $28.5D$ downstream from the center of the cylinder. The top and bottom boundaries were both placed at a distance of $12.5D$ from the cylinder.

Two different approaches for wall-modeling were simulated: (I) use of wall functions in a mesh with $y^+ \approx 30$ and 8.75×10^5 volumes, (II) solving the boundary layer in a mesh with $y^+ \approx 1$ and 1.4×10^6 volumes. Both were structured meshes with volumes elements, generated using Gmsh (Geuzaine and Remacle, 2009), an open source mesh generator. Figure 2 shows the three-dimensional mesh for the simulation with wall functions. The main difference between both meshes is related to refinement in the near-wall region as can be seen in Fig. 3. Sensitivity tests were conducted to determine the number of volumes in the spanwise direction and a value of 20 was chosen as compromise between accuracy and computational cost.

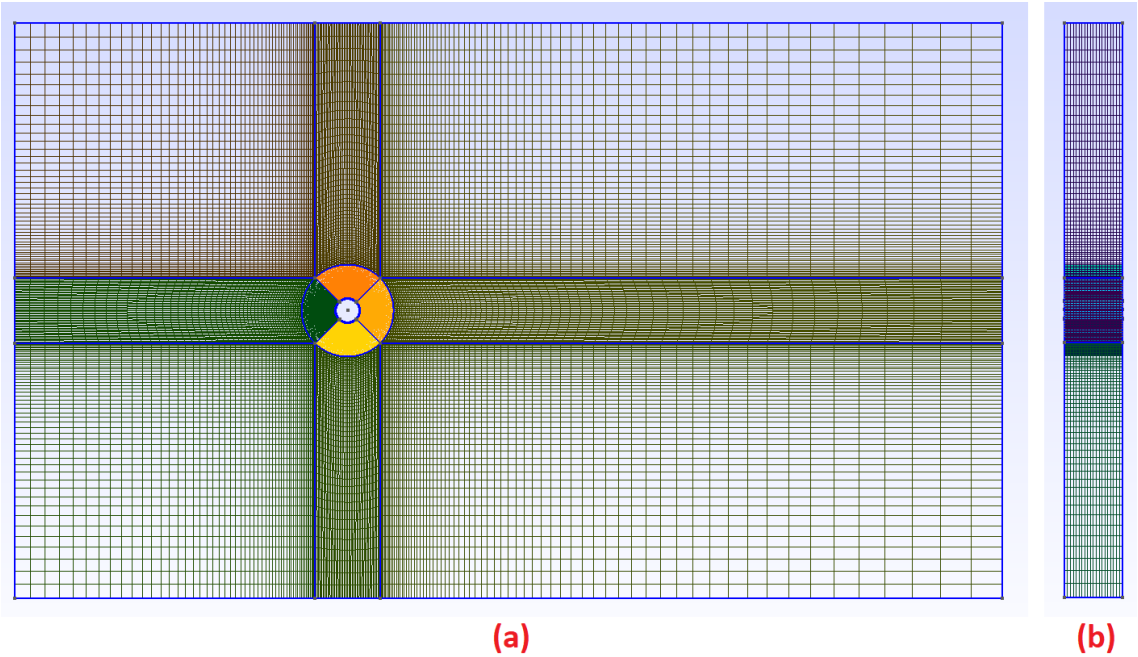

Figure 2: Three-dimensional mesh used for simulation with wall function treatment. (a) xy-plane view, (b) yz-plane view..

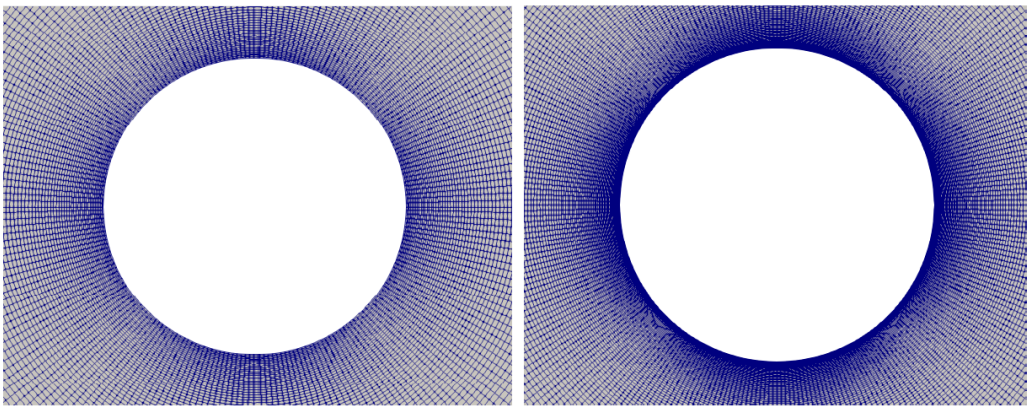

(a) Wall function treatment (b) Solving boundary layer treatment

Figure 3: Comparison of near-wall region refinement between mesh with $y^+ \approx 30$ (a) and $y^+ \approx 1$ (b).

2.3 Case B: Tandem Cylinders

For the cylinders in tandem arrangement, the same geometry defined by Lockard *et al.* (2007) was adopted, i.e. $D = 57.15$ mm, both separated by a distance of $3.7D$ between their centers. The Reynolds and Mach numbers were *Re* = 166,000 and $M = 0.127$, respectively. Regarding the computational domain, the distances between each boundary and the center of the upstream cylinder are: $13D$ for the inlet, top and bottom and $35D$ for the outlet. The spanwise extension is the same as in the experiments, which is $12.4D$.

Figure 4 depicts the three-dimensional mesh generated in Gmsh. It contains 5.9×10^6 volumes, with 60 cells in spanwise direction. Since the approach was to resolve the boundary layer, the mesh has $y^+ \approx 1$ for the volumes adjacent to the wall. Figure 5 shows the refinement in the near-wall region.

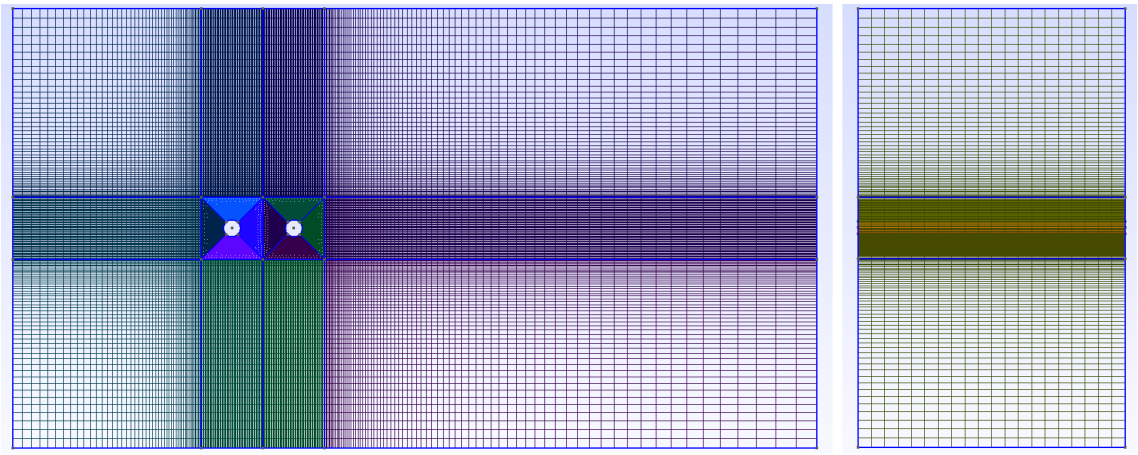

Figure 4: Three-dimensional mesh used for tandem cylinders case. (a) xy-plane view, (b) yz-plane view.

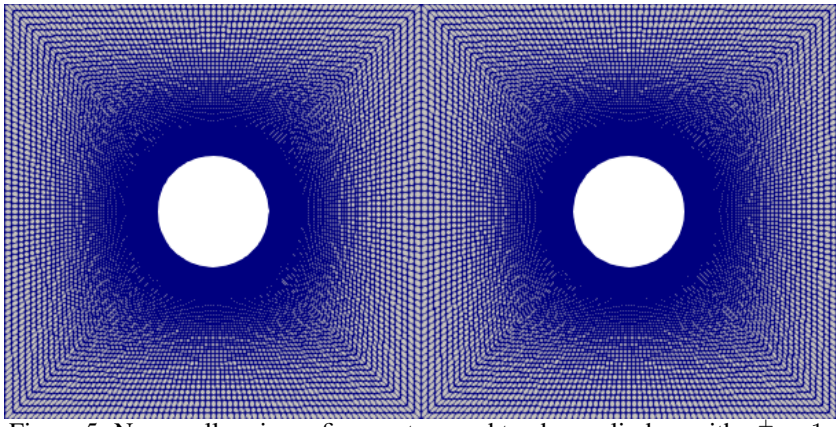

Figure 5: Near-wall region refinement around tandem cylinders with $y^+ \approx 1$.

2.4 Far-field Noise

For the far-field noise computations we used a dynamic library called libAcoustics, which is integrated with OpenFOAM and was developed by Epikhin *et al.* (2015); Ilya Evdokimov *et al.* (2020). This code is available for free download and contains acoustic analogies to be used in conjunction with CFD computations.

In this work, the Ffwocs-Willians and Hakings analogy (FW-H) (Ffowcs Williams and Hawkings, 1969) based on permeable surfaces was used to compute the far-field noise. In such approach, near field pressure and velocity data are stored on an arbitrary control surface, which should encompass the most significant sound-generating regions. This surface information is used as an input for the far-field noise computations. Particularly the Garrick Triangle (GT) formulation, described by Brès *et al.* (2010), was used as it shows increased computational efficiency for wind tunnel configurations.

Figure 6 shows the permeable surfaces used to collect aerodynamic data in both cases. The surfaces are three-dimensional and have the same spanwise extension as the domain. Figure 6(a) shows the surfaces for Case A, in which surface 1 extends 3*D* upstream, up and down from center of the cylinder and 10*D* downstream. Surface 2 has the same dimensions except for the streamwise length, extending up to 15*D* downstream.

Figure 6(b) depicts the surfaces for the tandem cylinders case. The distances from the center of the upstream cylinder to surface 1 are of 2*D* upstream, 2.5*D* up and down and 10*D* downstream. For surfaces 2,3 and 4, the downstream distances are 12.5*D*, 15*D* and 20*D*, respectively.

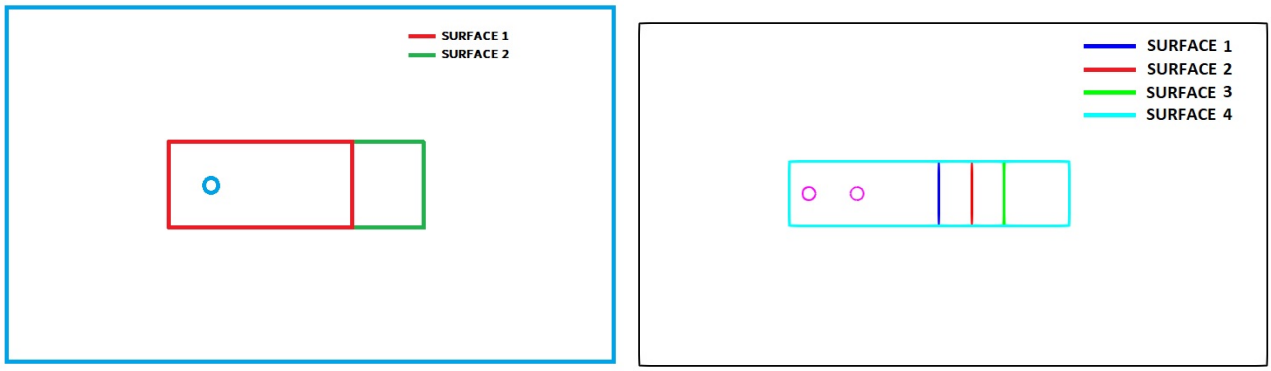

(a) (b)

Figure 6: FW-H surfaces inside the domain for (a) Cylinder case, (b) Tandem cylinders case.

Since the experiments conducted by Revell *et al.* (1978) used a cylinder of span length $12.7D$, whereas the simulated one has $2.5D$, a correction had to be applied before comparing the acoustic results for Case A. The correction used in this work is the same used by Orselli *et al.* (2009) in LES simulation. The method was proposed by Kato *et al.* (1993) and consists of adding a Sound Pressure Level (SPL) correction ($\Delta SPL_{corr}(\omega)$) to the SPL obtained numerically. This $\Delta SPL_{corr}(\omega)$ depends on the coherence length of the surface pressure fluctuations along the cylinder span, which changes with frequency. In addition, Curle's Analogy (Curle, 1955) was also used for noise computation. In this approach, the pressure field on solid surfaces, e.g. the surface of the cylinders, are used to predict far-field noise. In order to calculate only the surface integrals, the volume integrals are neglected. As consequence, only the noise due to dipole sources are computed.

For the acoustic field computations data was recorded during 0.1 s with same timestep as flow field simulation ($\Delta t = 1 \times 10^{-6}$ s for Case A and $\Delta t = 2.5 \times 10^{-6}$ s for Case B). Sampling frequency, that is given by the inverse of timestep, was 1000 kHz and 400 kHz for Cases A and B, respectively. The noise Power Spectral Density (PSD) spectrum was obtained using Fast Fourier Transform (FFT) algorithm, with resulting frequency resolution of 28.57 Hz. A Hanning window was employed with an overlap of 75% between blocks.

3. RESULTS

In order to validated the models, both wall-modeling approaches for the isolated cylinder - wall functions and resolving the boundary layer - were compared with experimental results of Revell *et al.* (1978). Those comparisons were separated into flow field and acoustic far-field data. For the tandem cylinders case, flow-field and acoustic far-field, results were compared with experimental data from Lockard *et al.* (2007).

3.1 Flow Field Results

Figure 7 shows the results for Case A, compared with experimental data, for the mean pressure coefficient on the cylinder surface. The position on the cylinder surface is determined by the angle relative to the stagnation point. Results for the wall-function approach show good agreement with experimental data, with larger deviations between 60° and 100°. On the other hand, the solving-boundary-layer approach underpredicted the pressure coefficient between 60° and 100° and over predicted the coefficients in the rear part of the cylinder. We should emphasize, however, that the experiment of Revell *et al.* (1978) used boundary layer trips in the region between 75° and 105° to force transition to turbulence. Our numerical approach considers a smooth cylinder with fully turbulent modeling. The possible effects of the trip, aligned with errors associated with using a shorter span and deficiencies of the turbulent model can be the main causes of the observed disparities.

Figure 8 show pressure coefficient data for Case B (tandem arrangement) compared to experimental results from Lockard *et al.* (2007). Good agreement between experimental and numerical results can be observed up to 100° for the upstream cylinder. However, results are underpredicted in the rear part of the cylinder, what can indicate deficiencies of the simulation to correctly predict separation and vortex-shedding dynamics. For the downstream cylinder, results also show good agreement with experimental data, with larger deviations in the rear part.

The mean drag coefficient ($\bar{C}_d$) computed for Case A along with the experimental value of Revell *et al.* (1978) are shown in Tab. 1. While the wall-function approach differed from the experiments by about 5%, the simulation resolving

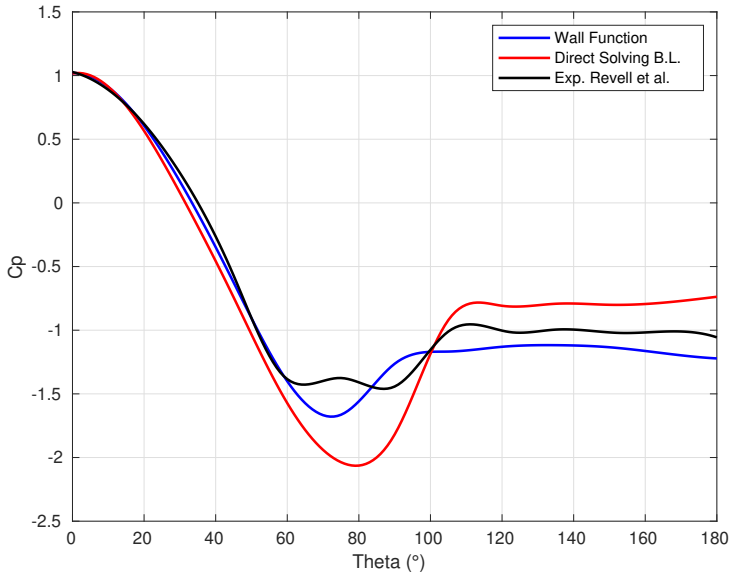

Figure 7: Mean pressure coefficient for numerical and experimental results of the isolated cylinder case.

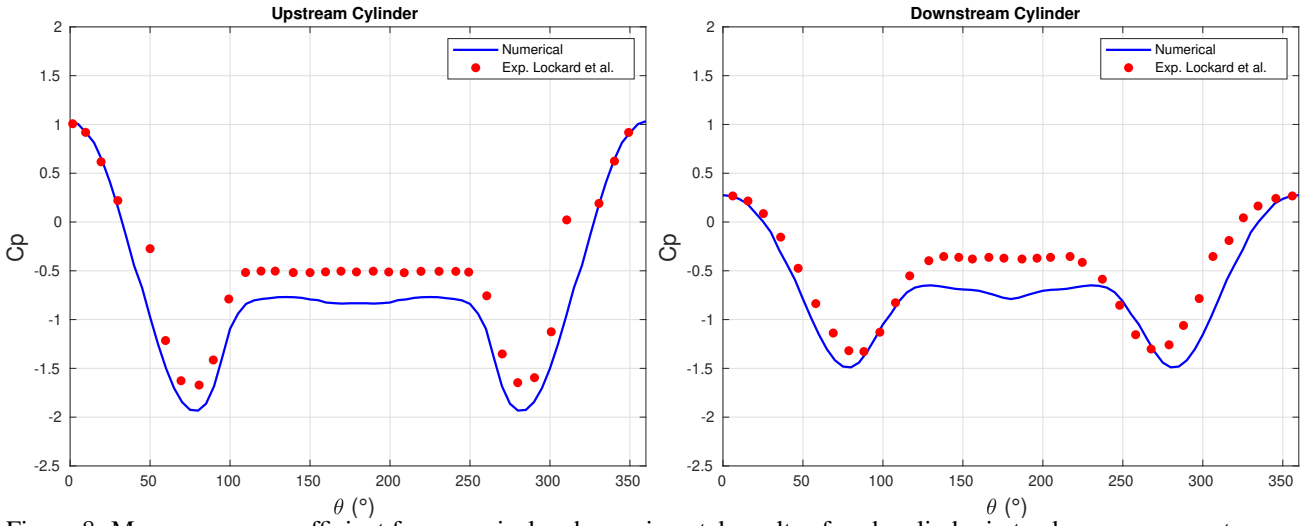

Figure 8: Mean pressure coefficient for numerical and experimental results of each cylinder in tandem arrangement case.

the boundary layer underpredicted the drag coefficient by about 36%. The reason for such large deviation could be still related to the differences between the tripped cylinder, from the experiments, and the simulated smooth cylinder.

The $\bar{C_d}$ data is also presented in Tab. 2 for Case B, and the comparison is done with experimental data from Neuhart *et al.* (2009). In this case, the drag coefficient was overpredicited by 4.6% for the upstream cylinder, and underpredicted by about 20% for the downstream cylinder. Although these deviations can be still significant, specially for the downstream cylinder, they are lower when compared to Case A.

Table 1: Mean coefficient drag ($\bar{C_d}$) for experimental and numerical results of cylinder case.

	$\bar{C_d}$
Experimental Revell *et al.* (1978)	1.07
Num. - wall functions	1.12
Num.- solving boundary layer	0.68

Table 2: Numerical mean coefficient drag ($\bar{C_d}$) comparison for upstream and downstream cylinders of tandem arrangement.

	C_d Upstream	C_d Downstream
Exp. Neuhart *et al.* (2009)	0.65	0.31
Numerical	0.68	0.37

3.2 Acoustic Field Results

As discussed earlier, a correction for the SPL was used due to differences between the simulated span length and the experimental setup. The correction was the same used by Orselli *et al.* (2009), which adds a value of ΔSPL_{corr} = 15.03 dB for the vortex shedding frequency and a value of ΔSPL_{corr} = 10.05 dB for other frequencies.

In order to analyse possible effects of spurious noise generated by vortexes crossing the downstream face of the FW-H surfaces, the downstream face was removed from some computations. The results from these surfaces, denominated open surfaces, are compared with results from the original, closed surfaces in Fig. 9. The PSD spectra obtained via Curle's analogy, is also included in the same figure. These results come from the simulation with solved boundary layer approach. Clearly, the FW-H closed surfaces show higher noise levels, for both surface lengths, when compared to open surfaces and to Curle's solid surface. Differences are greater for the shorter one, and possibly indicates spurious noise might be present. However, the open FW-H surfaces presented lower peak levels when compared to the Curle surface, which can imply that the removed face contained important information for the prediction of the peak value. More analyses need be conducted in future studies to understand this sensitivity to the surface definition.

Corrected numerical spectrum for the wall function approach - calculated using FW-H with two different open surfaces and using Curle's analogy with solid surface - and experimental sound spectrum obtained by Revell *et al.* (1978), for a tripped cylinder, are presented in Fig. 10. In this case, the original data from Revell *et al.* (1978) was corrected, taking into account the experimental bandwidth. Regarding numerical data, results of both open FW-H surfaces and Curle surface are compared. The only significant difference between both FW-H surfaces occurs in the first peak, where Surface 2 presented results 5 dB lower. Comparing numerical and experimental data, there is a clear mismatch between the frequencies of the peaks. Moreover, the peak values for FW-H surfaces were underpredicted by about 3 dB for Surface 1. On the other hand, Curle's analogy presented a good estimation of the peak value.

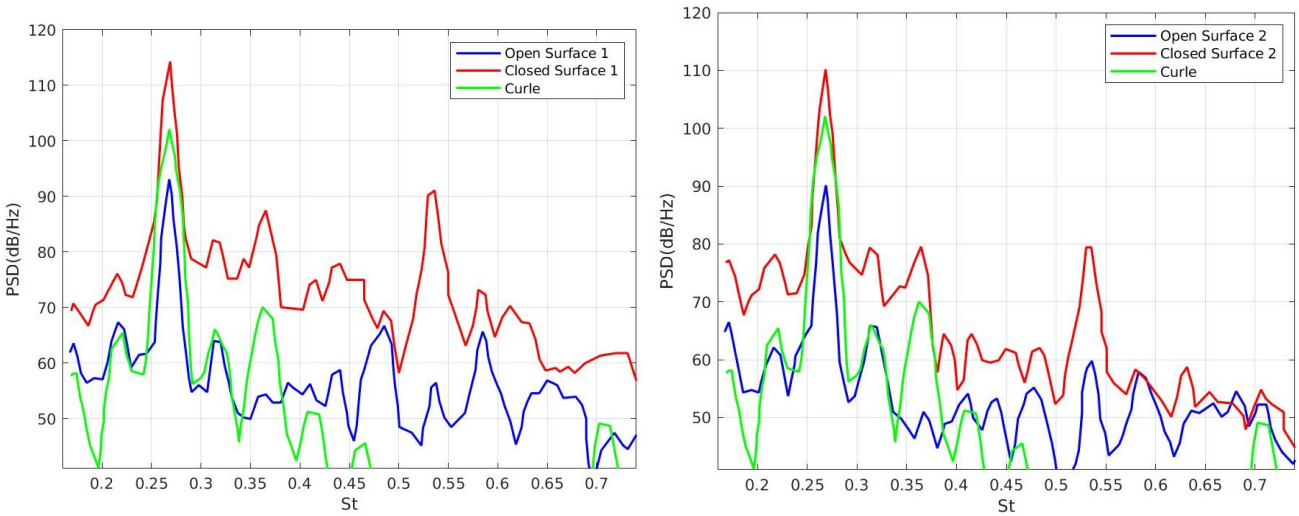

Figure 9: Comparison of open and closed FW-H surfaces (on the left, surface 1 and on the right, surface 2) with Curle surface.

The comparison between experimental data and the numerical results with resolved boundary layers is depicted in Fig. 11. The difference in the Strouhal (St) number of the first peak between numerical and experimental results is 0.026 (73 Hz). Amplitudes predicted by FW-H surfaces were approximately 9 dB below the experimental value. For Curle surface the amplitude difference is only 0.8 dB above experimental.

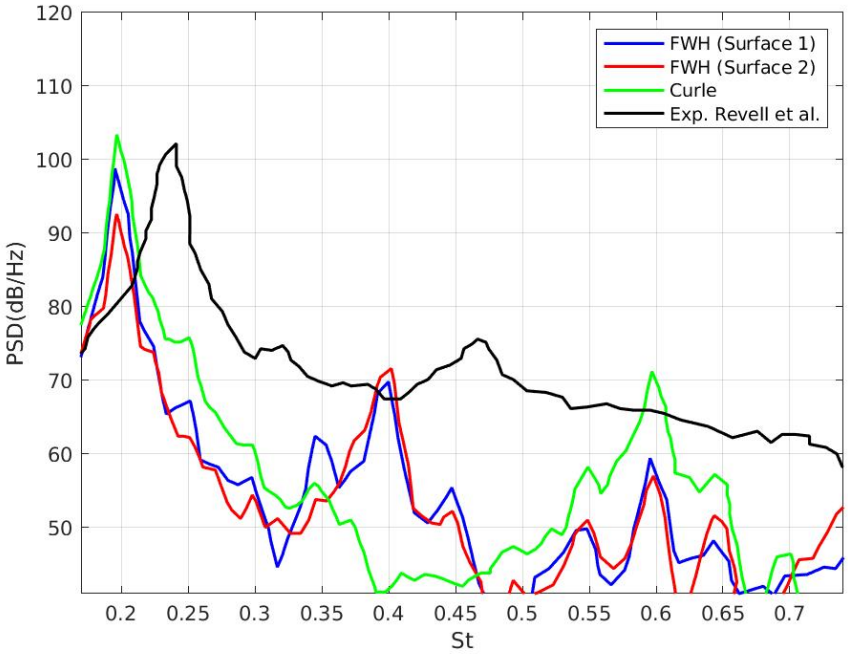

Figure 10: Noise spectrum comparison between the wall-function approach and experimental data for Case A.

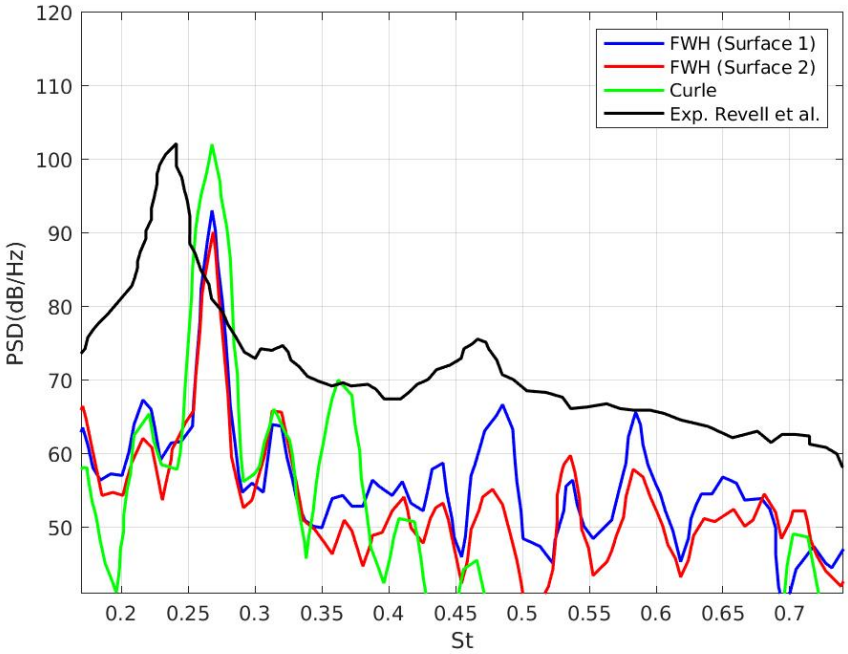

Figure 11: Noise spectrum comparison between numerical with solved boundary layer approach and experimental data for Case A.

Noise spectra for case B, presented in Fig. 12 for closed and open surfaces, were calculated for the far-field point (-8.33D, 27.815D). Results are compared to experimental data from Lockard *et al.* (2007) and no SPL correction was required, since the total spanwise length of the cylinder was simulated. The St value of the first peak was well estimated by the numerical model. Computations with closed Surface 1 (Fig.. 12 (a)) presented maximum levels about 1-2 dB when compared to the experimental data. However, when longer surfaces are considered, the predicted peak value is lower (about 92 dB for surfaces 2 and 4).

Still regarding the first peak, although results for closed surfaces 2 and 4 are very close to each other, surface 3 presented considerably lower levels. Despite the observed sensitivity to the surface size, levels for surfaces 2 and 4 are consistent with Curle's analogy and show good agreement with experimental data. When open surfaces are taken into account (Fig.. 12 (b)), the spectra from all the different FW-H surfaces show very similar levels. Nevertheless, the first tone level was underestimated with respect to the Curle surface and experiments. These deviations could be related the loss of the downstream face contribution to the acoustic field.

It is clear that results show considerable sensitivity to the position of the downstream face of the FW-H surface. The reason for these disparities between different closed surfaces and open surfaces are not clear and further analyses are required. Regarding Curle's analogy, the first tone value was underestimated by about 1 dB. Moreover, only this approach could reasonably reproduce the St and amplitudes of the second and third peaks.

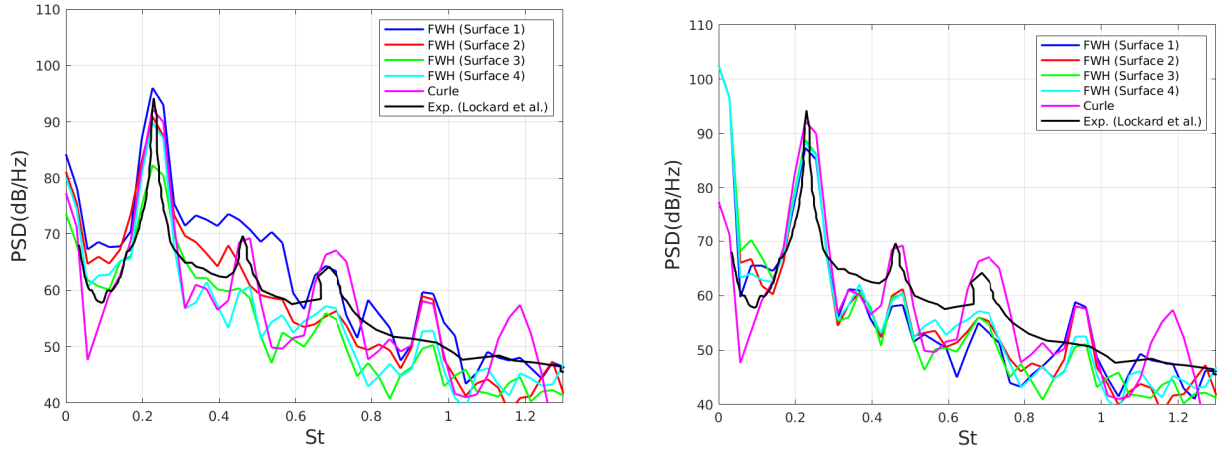

(a) Closed Surfaces (b) Open Surfaces

Figure 12: Noise spectrum comparison between numerical results and experimental data for the tandem cylinders case.

4. CONCLUSIONS

This work analysed the noise generated by cylinders in uniform flow using the opensource code OpenFOAM, coupled with the LibAcoustics tool. Validation was conducted by comparisons with experimental data for one cylinder (case A) and cylinders in tandem arrangement (case B).

Regarding aerodynamic data, results were in good agreement with experimental data for the pressure coefficient. Disparities can be related to inaccuracies in the prediction of the separation point by the used turbulence models. Moreover, for case A, differences between in the numerical model and experimental setup, such as the span wise length and the use of a boundary layer trip, could also be a cause of the observed deviations.

Farfield noise was computed with FW-H surfaces of different sizes, with open and closed ends. Results showed sensitivity to the size of the surface and more analyses are needed to define a suitable surface size. In general, results for case B agreed better with experiments than case A, both in the prediction of the frequency of peaks and their amplitude. Such deviations in the prediction of peaks are usually observed for URANS simulations with reduced span in the literature. For case A, the use of a correction on SPL to account for the reduced span, is also a source of in certainties. Overall improvements are needed in the simulation models, which will be addressed in future works.

5. ACKNOWLEDGEMENTS

Simulations were conducted using the cluster of LabCC- Laboratório de computação científica, CTJ-UFSC.

6. REFERENCES

Brès, G.A., Pérot, F. and Freed, D., 2010. "A ffowcs williams-hawkings solver for lattice-boltzmann based computational aeroacoustics". In *Proceedings of the 16th AIAA/CEAS Aeroacoustics Conference - AIAA 2010*. Stockholm.

Curle, N., 1955. "The influence of solid boundaries upon aerodynamic sound". *Proceedings of the Royal Society of London*, , No. 231 A, pp. 505–517.

Epikhin, A., Evdokimov, I., Kraposhin, M., Kalugin, M. and Strijhak, S., 2015. "Development of a dynamic library for computational aeroacoustics applications using the openfoam open source package". *Procedia Computer Science*, Vol. 66, pp. 150–157.

Ergin, S. and Bulut, S., 2017. "Estimating flow-induced noise of a circular cylinder using numerical and analytical acoustic methods". In *Proceedings of the 17th International Maritime Association of the Mediteranean - IMAM 2017*. Lisbon.

Ffowcs Williams, J.E. and Hawkings, D.L., 1969. "Sound generation by turbulence and surfaces in arbitrary motion". *Philosophical Transactions of the Royal Society of London. Series A, Mathematical and Physical Sciences*, Vol. 264, No. 1151, pp. 321–342. ISSN 00804614.

Geuzaine, C. and Remacle, J.F., 2009. "Gmsh: a three-dimensional finite element mesh generator with built-in pre- and post-processing facilities". *International Journal for Numerical Methods in Engineering*, Vol. 79, No. 11, pp. 1309–1331.

Jenkins, L.N., Khorrami, M.R., Choudhari, M.M. and McGinley, C.B., 2005. "Characterization of unsteady flow structures around tandem cylinders for component interaction studies in airframe noise". In *Proceedings of the 11th AIAA/CEAS Aeroacoustics Conference - AIAA 2005*. Monterey.

Kato, C., Iida, A., Takano, Y., Fujita, H. and Ikegawa, M., 1993. "Numerical prediction of aerodynamic noise radiated from low mach number turbulent wake". In *Proceedings of the 31st Aerospace Sciences Meeting - AIAA 93*. Reno.

llya Evdokimov, UniCFD and Epikhin, A., 2020. "unicfdlab/libacoustics: Openfoam+ v1912 version of libacoustics". doi:10.5281/zenodo.3878439.

Lockard, D.P., Khorrami, M.R., Choudhari, M.M., Hutcheson, F.V., Brooks, T.F. and Stead, D.J., 2007. "Tandem cylinder noise predictions". In *Proceedings of the 13th AIAA/CEAS Aeroacoustics Conference - AIAA 2007*. Rome.

Menter, F.R., 1994. "Two-equation eddy-viscosity turbulence models for engineering applications". *AIAA Journal*, Vol. 32, No. 8, pp. 1598–1605.

Neuhart, D., Jenkins, L., Choudhari, M. and Khorrami, M., 2009. *Measurements of the Flowfield Interaction Between Tandem Cylinders*. doi:10.2514/6.2009-3275.

OpenCFD, 2020. "Openfoam: the open source cfd toolbox user guide". OpenCFD Ltd, https://www.openfoam.com/documentation/overview. Accessed 17 June 2021.

Orselli, R.M., Meneghini, J.R. and Saltara, F., 2009. "Two and three-dimensional simulation of sound generated by flow around a circular cylinder". In *Proceedings of the 15th AIAA/CEAS Aeroacoustics Conference - AIAA 2009*. Miami.

Revell, J.D., Prydz, R.A. and Hays, A.P., 1978. "Experimental study of aerodynamic noise vs. drag relationships for circular cylinders". *AIAA Journal*, Vol. 16, No. 9, pp. 889–897.

Ruijgrok, G.J.J., 1993. *Elements of aviation acoustics*. Delft University Press, Delft.

Seo, J.H. and Moon, Y.J., 2007. "Aerodynamic noise prediction for long-span bodies". *Sound and Vibration*, Vol. 306, pp. 564–579.

Zdravkovich, M.M., 1985. "Flow induced oscillations of two interfering circular cylinders". *Journal of Sound and Vibration*, Vol. 101, No. 4, pp. 511–521.